Author/s:
Zhang, B;Lyskov, I;Wilson, LJ;Sabatini, RP;Manian, A;Soleimaninejad, H;White, JM;Smith, TA;Lakhwani, G;Jones, DJ;Ghiggino, KP;Russo, SP;Wong, WWH

Title:
FRET-enhanced photoluminescence of perylene diimides by combining molecular aggregation and insulation

Date:
2020-07-14

Citation:
Zhang, B., Lyskov, I., Wilson, L. J., Sabatini, R. P., Manian, A., Soleimaninejad, H., White, J. M., Smith, T. A., Lakhwani, G., Jones, D. J., Ghiggino, K. P., Russo, S. P. & Wong, W. W. H. (2020). FRET-enhanced photoluminescence of perylene diimides by combining molecular aggregation and insulation. Journal of Materials Chemistry C, 8 (26), pp.8953-8961. https://doi.org/10.1039/d0tc02108c.

FRET-Enhanced Photoluminescence of Perylene Diimides by Combining Molecular Aggregation and Insulation

Bolong Zhang[a,b], Igor Lyskov[d], Lachlan J. Wilson[a], Randy P. Sabatini[c], Anjay Manian[d], Hamid Soleimaninejad[a,f], Jonathan M. White[e], Trevor A. Smith[a], Girish Lakhwani[c], David J. Jones[b], Kenneth P. Ghiggino[a,b], Salvy P. Russo[d*] and Wallace W. H. Wong[a,b*]

Abstract: The photoluminescence quantum yield (ϕ_{PL}) of perylene diimide derivatives (PDIs) is often limited by aggregation caused quenching (ACQ) at high concentration or in the neat solid-state. Energy transfer in high dye concentration systems is also a key factor in determining ϕ_{PL} as a result of energy funneling to trap sites in the sample. By tuning the substituents, we present two classes of PDIs with aggregation and insulation of the PDI core. By combining these fluorophores in a polymer film, we demonstrate highly emissive samples (85% ϕ_{PL}) at high concentration (140 mM or 20 %w/w). Experimental and theoretical studies provide insight into why such a combination is necessary to achieve high ϕ_{PL}. While insulated fluorophores maintain respectable ϕ_{PL} at high concentration, an improved ϕ_{PL} can be achieved in the presence of appropriately oriented fluorophore aggregates as emissive traps. The theoretical calculations show that the relative orientation of aggregated monomers can result in energetic separation of localized states from the charge-transfer and bi-excitonic states thereby enabling high ϕ_{PL}.

Introduction

In many technological applications, such as light emitting diodes[3]/transistors,[4] optically-pumped lasers,[5] luminescent solar concentrators,[6-8] and artificial light-harvesting antennae,[5] aggregation caused quenching (ACQ)[9, 10] can negatively impact device performance. Many organic fluorophores exhibit a photoluminescence quantum yield (ϕ_{PL}) close to unity in dilute solution,[11] but it is difficult to achieve a high ϕ_{PL} at high concentration or in the aggregated state.[12-14] A high ϕ_{PL} is an essential criterion for designing advanced fluorophores for the above-mentioned applications and thus the development of materials with high tolerance to ACQ is an important scientific challenge.

Although the phenomenon of aggregation induced emission in some materials can lead to high emission in the aggregated form,[15, 16] the ϕ_{PL} can still be far from unity in the solid-state.[17, 18] The other strategy to avoid ACQ is to build steric hindrance around the fluorophore, also called molecular insulation.[1, 19, 20] The steric hindrance will reduce intermolecular interaction between the fluorophores when they form aggregates, leading to reduction of ACQ and higher ϕ_{PL} under high concentration conditions. Several reported studies have demonstrated this molecular insulation strategy.[21-24]

Perylene diimide (PDI) derivatives are a class of organic fluorophores that are widely-used in research and as commercial dyes due to their good photo-stability, tunable chemical structure and potential for high ϕ_{PL}.[11] Many PDI derivatives have close to unity ϕ_{PL} in dilute solutions but the ϕ_{PL} can be significantly reduced in concentrated solution or in the neat solid-state.[1, 25, 26] As the planar perylene core tends to associate through π-π stacking, the ACQ effect often leads to ϕ_{PL} reduction when the concentration is increased.[27, 28] Molecular insulation has proved an effective approach to restore the ϕ_{PL} of many organic fluorophores including PDIs[19, 29, 30], providing steric hindrance. This decreases association of the perylene cores, thus reducing the quenching interaction among molecules.

The design and synthesis of molecularly insulated PDI derivatives by installing bulky-substituents on the imide-position of the perylene core was reported in our previous study (Figure 1a).[1] It was found that core-core interaction was present even in the most insulated compound in that series (bPDI-3) which showed aggregate emission in neat amorphous films. Interestingly, two other derivatives, bPDI-2 and bPDI-4, showed a greater amount of aggregate emission and higher ϕ_{PL}.[1] We hypothesized that energy transfer contributed to a reduction of ϕ_{PL} at high concentration. The energy migration process does

[a.] *ARC Centre of Excellence in Exciton Science, School of Chemistry, The University of Melbourne, VIC 3052, Australia.*
[b.] *Australian Centre for Advanced Photovoltaics, School of Chemistry, The University of Melbourne, Parkville, Victoria, 3010, Australia.*
[c.] *ARC Centre of Excellence in Exciton Science, School of Chemistry, and The University of Sydney Nano Institute, The University of Sydney, NSW 2006, Australia.*
[d.] *ARC Centre of Excellence in Exciton Science, School of Science, RMIT University, Melbourne, Victoria 3000, Australia*
[e.] *School of Chemistry, Bio21 Institute, The University of Melbourne, 30 Flemington Road, Parkville, Victoria, 3010, Australia.*
[f.] *Biological Optical Microscopy Platform (BOMP), Bio21 Institute Node, The University of Melbourne, Parkville, Victoria 3010, Australia*

† E-mail: wwhwong@unimelb.edu.au; salvy.russo@rmit.edu.au
Electronic Supplementary Information (ESI) available: [details of any supplementary information available should be included here]. See DOI: 10.1039/x0xx00000x

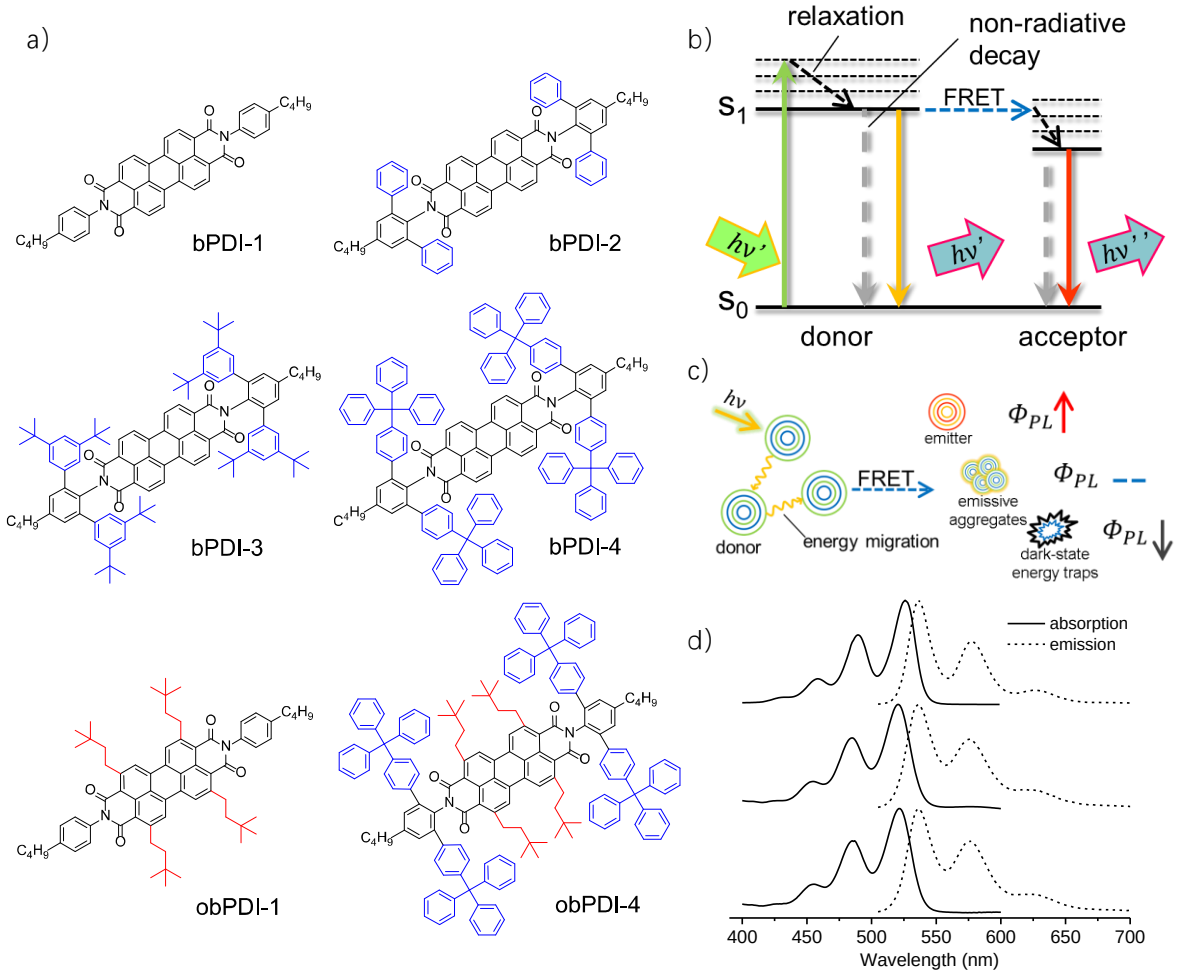

Figure 1. a) The chemical structure of all PDI derivatives. The imide substituents are highlighted blue while the ortho-substituents are red. bPDI-1, 2, 3 and 4 have been reported previously.[1] b) Simple Jablonski diagram illustrating the FRET process which requires a certain proximity of fluorophores or high concentration of bPDIs. c) Illustration of possible FRET acceptors: single emitters, emissive aggregates and non-emissive aggregates. d) The absorption and emission spectra (λ_{ex}= 490 nm) of the bPDIs (bPDI-3 for example), obPDI-1 and obPDI-4 recorded in dilute solution conditions.

not directly cause any ϕ_{PL} loss, but it increases the likelihood of energy trapping by low concentrations of any non-emissive species present. The strongly overlapped absorption and emission spectra of the PDI derivatives meant that Förster resonance energy transfer (FRET)[31, 32] was efficient in high concentration samples (Figure 1b).[1, 19, 33] Therefore, only a small amount of non-emissive energy trap was required to significantly reduce ϕ_{PL}.

On the other hand, energy transfer can sometimes assist in maintaining high ϕ_{PL} by rapidly funneling the energy to a highly emissive acceptor thus bypassing energy loss pathways.[1] This phenomenon has often been observed in donor-emitter fluorophore systems across both organic and inorganic materials.[34-36] The ϕ_{PL} of bPDIs were significantly improved when highly emissive energy acceptors (e.g. Lumogen Red 305) were introduced into the system (**Figure 1c**).[1, 8, 19]

In this work, we designed two new PDI derivatives with the intention to improve molecular insulation. The photophysical properties in dilute solution as well as in polymer and neat films were investigated. Time-resolved fluorescence spectroscopy was used to study the energy transfer process in the high concentration polymer samples. Quantum chemical calculations were performed to understand how the structure of PDI aggregates affects the ϕ_{PL}. Lastly, a small amount of emissive aggregate was blended with a fully insulated PDI derivative, resulting in the best ϕ_{PL} at high concentration in polymer films.

Results and discussion

Spectroscopic characterization

Inspired by the side-by-side molecular packing of bPDI-4 in its crystal form[1], we have designed and synthesized two ortho-substituted bPDIs, obPDI-1 and obPDI-4 (Figure 1a). The structure of obPDI-1 is conducive to π - π stacking and H-aggregation, while the structure of obPDI-4 is designed to provide complete molecular insulation and thus prevent aggregation.

Both obPDI-1 and obPDI-4 were synthesized by a one-step Ru-catalyzed direct-alkylation reaction with 1,3-dimethylbutene from bPDI-1 and bPDI-4 (synthesis and characterization details are provided in the ESI).[37] As both the absorption and emission spectra of obPDI-1 and obPDI-4 in dilute solution are identical to the previously reported bPDIs (<5 nm spectral shift, Figure 1d), the imide- and ortho-position substituents have no notable influence on the photophysical properties of the perylene core. In a poly(methyl methacrylate) (PMMA) thin-film matrix (both 10 mM and 120 mM, Figure 2a), the absorption spectra of obPDI-1 showed a change in relative height of the vibronic band structure and a red shift of the peak at the longest wavelength compared to the dilute solution case, suggesting the formation of hybrid H- and J-aggregates. The emission of obPDI-1 was significantly red-shifted at 10 mM in PMMA and became dominated by aggregate emission at 10 mM, 120 mM and in the amorphous solid-state, due to the emergence of emissive aggregates. The perylene core of obPDI-4 was sterically well protected. This was reflected in the absorption spectrum that remained unchanged at all concentrations while the emission spectrum was only slightly perturbed at 120 mM in PMMA and retained clear vibronic structure in the amorphous solid-state(Figure 2b). The ϕ_{PL} values of obPDI-1 and obPDI-4 in dilute solution were both above 90%, indicating that the ortho-substituents did not lead to any non-emissive energy loss in comparison with the other bPDIs. At a concentration of 10 mM in the PMMA matrix, the ϕ_{PL} values of the obPDIs were ~10% lower compared to dilute solution. Surprisingly, the ϕ_{PL} of the fully molecularly insulated obPDI-4 at 120 mM was only 40%, which is lower than the ϕ_{PL} of obPDI-1 at 56% (Table S1, see measurement details in **ESI**). The ϕ_{PL} variation of obPDIs with concentration was not consistent with that expected based on the ACQ effect alone.

Time-resolved spectroscopy

A series of time-resolved spectroscopy experiments were performed to study the unexpected ϕ_{PL} variation (Table S1). In dilute solution, the emission decays of both obPDI-1 and obPDI-4 were both non-exponential with the amplitude average fluorescence lifetimes of ~4 ns, which is typical of PDI derivatives. The average fluorescence lifetime of obPDI-1 increased to 10.35 ns at 10 mM in PMMA matrix, suggesting aggregate formation with increasing concentration.[38] When the concentration of obPDI-1 and obPDI-4 increased to 120 mM and in neat solid-state samples, the fluorescence decays of both decreased substantially, typical of ACQ. The observation of the fluorescence lifetime variation in obPDIs agrees with the ϕ_{PL} variation at different concentrations.

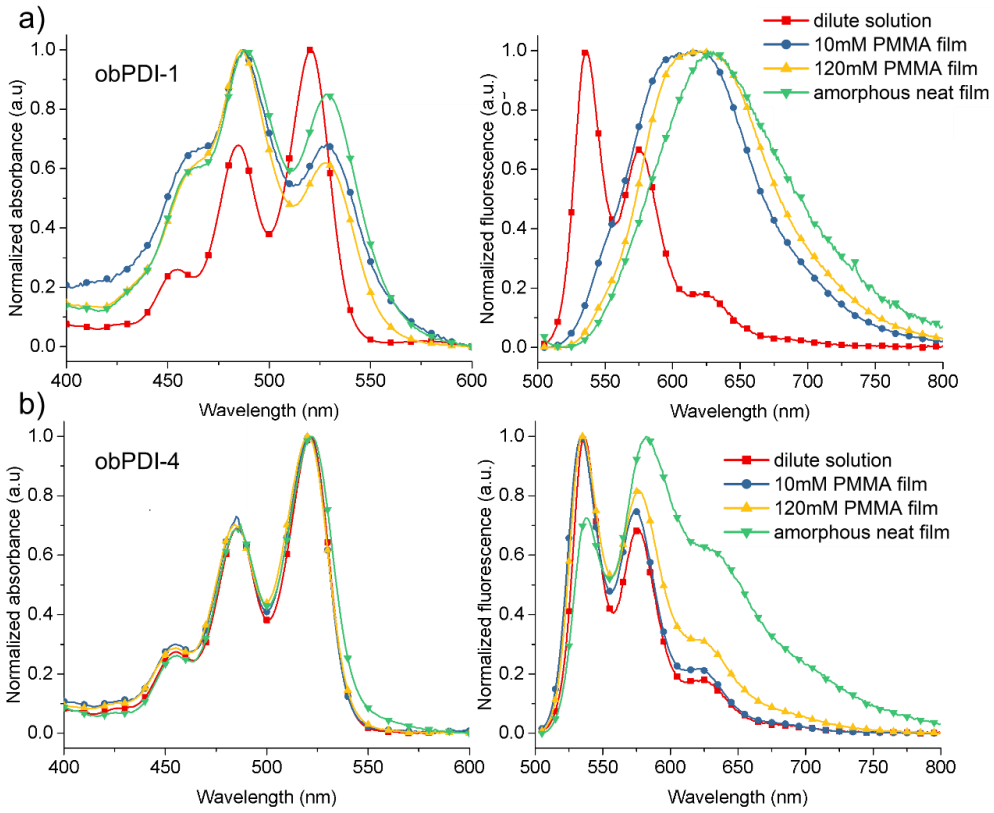

Figure 2. Absorption (left) and emission (right) spectra of a) obPDI-1 and b) obPDI-4 at a range of concentrations (λ_{ex}= 490 nm).

Singular value deconvolution (SVD)[39, 40] analysis, using the multivariate curve resolution alternating least-squares (MCR-ALS) algorithm,[38, 41] was performed on the fluorescence decays collected as a function of emission wavelength for both obPDI-1 and obPDI-4 in order to further investigate the influence of aggregation and molecular insulation. The SVD of the time-resolved fluorescence data of obPDI-1 and obPDI-4 at 120 mM suggested that two components contribute to the overall emission spectra, i.e. the monomeric component and the red-shifted aggregated component (Figure 3a and b). The temporal deconvolution suggested the fluorescence of the aggregated components in general occurs over longer timescales than the corresponding monomer component. For obPDI-4, the fractional contribution of the monomer component (72%) to the overall decay was much higher in comparison to the aggregated component (28%), again suggesting that obPDI-4 is highly sterically-hindered and there is little opportunity to form any emissive aggregates. On the other hand, the fluorescence of obPDI-1 at 120 mM was mainly from the aggregated component (86%), which significantly increases the overall fluorescence lifetime of obPDI-1.

The details of the exponential fitting to the temporal decomposition are listed in Table S2. For obPDI-1, both the monomeric and the aggregated component started to decay right after the excitation, but the decay of the monomeric fluorescence is much faster than the aggregated fluorescence. This could be a result of energy transfer from component 1 to component 2. The abundance of ground state aggregate species as seen in the absorption spectrum in Figure 2a meant that component 2 emission mainly stems from direct photoexcitation of aggregates. Since the aggregated component of obPDI-1 was highly emissive, the fluorescence lifetime in 120 mM was quite long and the overall ϕ_{PL} higher than obPDI-4. This interesting property of obPDI-1 is further discussed in the theoretical section below.

For obPDI-4, a growth in the emission intensity of component 2 is seen prior to it decaying. Since the growth rate of component 2 (τ_g = 0.35 ns) was similar to the shorter decay (τ_1 = 0.25 ns) of component 1 (Table S2), the excitation of the aggregates is interpreted as mainly coming from the partial quenching of the monomeric emission. It is noteworthy that the monomeric fluorescence was still dominant (72%). The overall fluorescence lifetime of obPDI-4 in 120 mM at 1.58 ns (Table S1) was much shorter than in dilute solution (3.89 ns) indicating both components of obPDI-4 may be further quenched by non-emissive energy traps. These time-resolved spectroscopy results are consistent with the lower than expected ϕ_{PL} for obPDI-4.

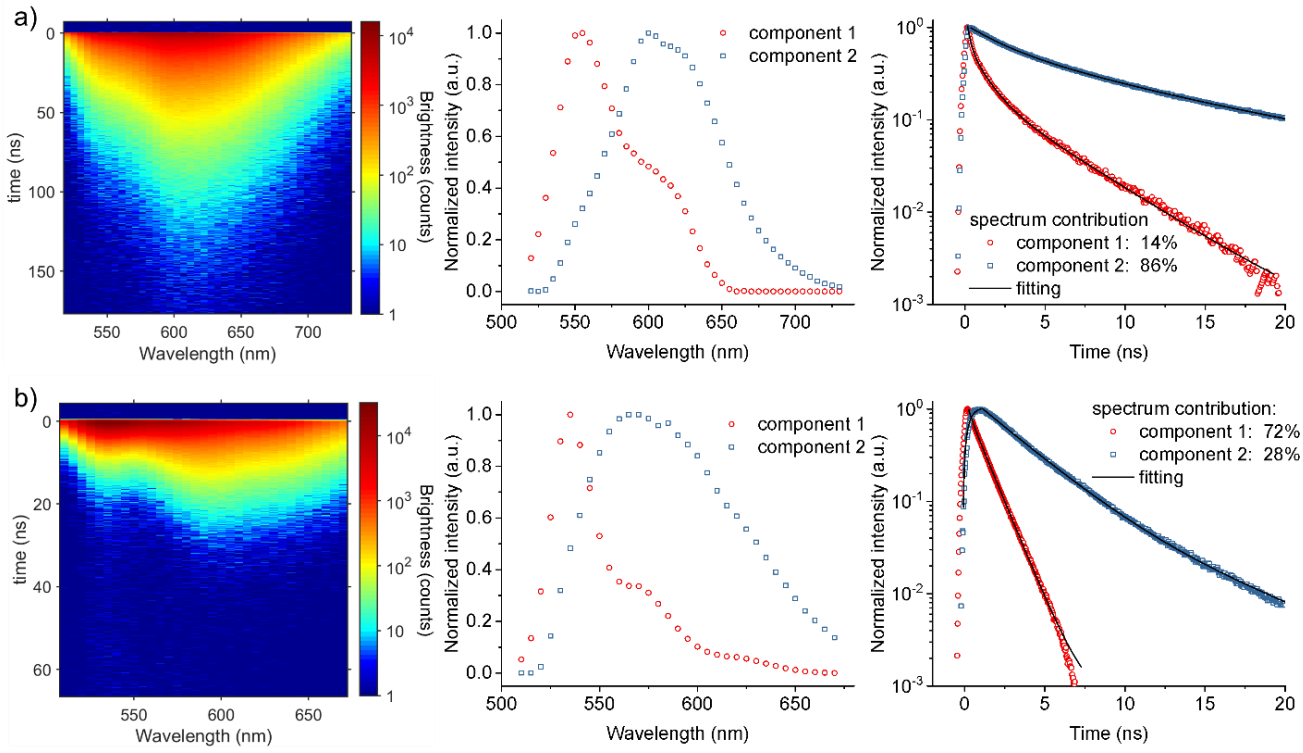

Figure 3. The time-resolved fluorescence data of a) obPDI-1and b) obPDI-4 at 120 mM in PMMA matrix together with the spectral and temporal deconvolution via MCR-ALS. Components 1 and 2 are assigned to the monomeric and aggregated fractions of emission respectively.

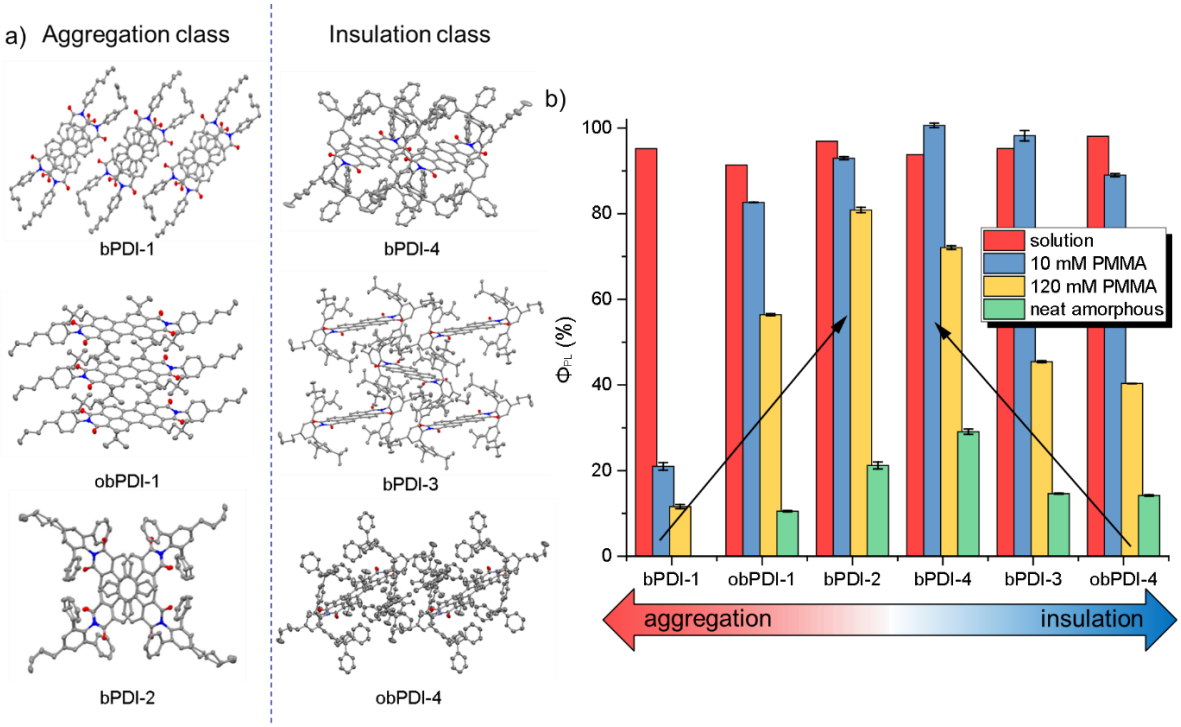

Figure 4. a) The crystalline packing of bPDI-1, obPDI-1 and bPDI-2 shows clear π- π stacking among molecules, but the packing arrangements are different. However, the crystalline packing of bPDI-4, bPDI-3 and obPDI-4 indicated the bulky-substituents prevented any possibility of π- π stacking among these molecules. The crystallography data of the bPDIs are provided in the Supporting Information for detailed viewing. b) The ϕ_{PL} of all six PDIs under different conditions. The PDIs with hybrid characteristics of molecular aggregation and insulation in general exhibit higher ϕ_{PL} values in this series. The $\phi_{PL}$of the solution sample was measured by the relative method using perylene orange (ϕ_{PL} 99%) as the reference and the solid-state samples were measured by the absolute method using an integrating sphere (averaging over 3 measurements). The uncertainty of the relative and absolute ϕ_{PL}measurement are ~6.0% and 5.5% respectively.[2]

Comparison of six bPDI and obPDI derivatives

The entire bPDI series, including obPDI-1 and obPDI-4, were then compared to map the influence of the aggregation and molecular insulation on the ϕ_{PL}. The X-ray crystal packing data (Figure 4a) was used to separate the bPDIs into two classes, i.e. an aggregation class and an insulation class. As shown in Figure 4a, bPDI-1, obPDI-1 and bPDI-2 belong to the aggregation class, because these molecules exhibit π−π stacking, indicating a strong interaction between the perylene cores. The stacking patterns of the three compounds exhibit a different angle between neighboring molecules, due to the imide-position or ortho-position substituents. In contrast, the molecular insulated class, namely bPDI-4, bPDI-3 and obPDI-4, showed no direct interaction between the perylene cores, due to the steric hindrance from the bulky substituents.

The absorption and emission spectra of all the bPDIs (Figure 2 and S5) at high concentration in the PMMA matrix are consistent with the assignments made from the crystal packing of the materials. For the aggregation class, the absorption spectra of bPDI-1 were blue-shifted at 10 mM, 120 mM and in the neat solid-state (Figure S5a), indicating H-type aggregate formation[42, 43] at high concentration, while that of obPDI-1 showed changes indicative of mixed H- and J-aggregate formation as discussed earlier (Figure 2a). The absorption spectrum of bPDI-2 was slightly red-shifted and broadened, again indicative of aggregation (Figure S5b). The emission spectra of the aggregation class were all red-shifted, suggesting the fluorescence was dominated by aggregate emission. For the insulation class, the absorption spectra of bPDI-4, bPDI-3 and obPDI-4 at high concentration in PMMA matrix or in the neat solid-state were all identical to the spectra recorded in dilute solution, indicating monomeric species dominated. The emission spectra of the insulation class showed much less influence from the aggregate species at high concentration. Even in the neat solid-state, the emission spectra retained some characteristics of the monomeric species. bPDI-4 showed the most aggregate emission in the insulation series at 120 mM in PMMA matrix.

As shown in Figure 4b, the ϕ_{PL} of the PDIs were all above 90% in dilute solution, indicating that the bulky substituents did not have any significant direct influence on the quantum efficiency of the perylene cores. In the absence of bulky substituents, bPDI-1 formed aggregates readily and the ϕ_{PL} dropped to 20% at 10 mM while all other PDIs showed ϕ_{PL} above 80% under the same conditions. However, at 120 mM in PMMA matrix, the ϕ_{PL} varied significantly depending on the molecular structure and the degree of molecular insulation. Surprisingly two of the most molecularly insulated PDIs, i.e. bPDI-3 and obPDI-4, showed ϕ_{PL} values that were much lower than the less sterically hindered bPDI-2 and bPDI-4. On the other hand, the strongly aggregated obPDI-1 also showed higher ϕ_{PL} compared to bPDI-3 and obPDI-4 at 120 mM. This indicated that the ACQ effect was not the dominant process affecting the ϕ_{PL} of PDIs at high concentration in PMMA.

As mentioned previously, bPDI-4 displayed more aggregate emission at 120 mM in the insulation class of bPDIs. Since the

ϕ_{PL} of bPDI-4 at 120 mM was much higher than bPDI-3 and obPDI-4, one can conclude that the ϕ_{PL} of the aggregate component for bPDI-4 was above the molecularly insulated PDIs at this concentration. To date, the ACQ effect was pervasive for bPDIs, but the formation of emissive aggregates in bPDI-4 provided an alternative pathway that helped to restore the ϕ_{PL}. The energy transfer process allowed a small amount of the emissive aggregates to substantially change the ϕ_{PL} of PDIs. The ϕ_{PL} values were lower in the insulation class with less aggregate emission observed at high concentration or in neat films.

Quantum Chemical Calculations

The above experiments suggest that the presence of emissive aggregate species is a key factor in achieving a high ϕ_{PL} for PDI derivatives at high concentration. In addition to the localized states (L), molecular clusters can give rise to low-lying charge-transfer states (CT), which lead to trap states in PDI aggregates.[44, 45] Furthermore, spin conversion from singlet to triplets via intersystem crossing or singlet fission can promote nonradiative deactivation and, hence, inevitably reduce ϕ_{PL}. Therefore, in order to further understand the relationship between the structural nature of the bPDI aggregates (bPDI-1, obPDI-1, bPDI-2) and ϕ_{PL}, we performed a series of quantum chemical calculations. The multi-reference DFT/MRCI-R2016[46] method was employed, which is well-suited for bichromophoric systems providing an accurate description of excited states with double excitation character. In particular, the possible contributions of CT and correlated-triplet-pair (TT) states to fluorescence quenching in these aggregates were explored. For each pair of chromophores, the relative orientation of the monomers was taken from the experimental X-ray diffraction data. To understand the excitonic character of the singlet excited states, the one-particle transition density matrix analysis of the supramolecular DFT/MRCI wavefunction was performed.[47] This enables the partitioning of the exciton density into 4 constituent components which are labelled ω_{AA}, ω_{BB}, ω_{AB} and ω_{BA}. The components ω_{AA} and ω_{BB} represent the probability of an exciton residing on the respective monomers (A or B), i.e. realizing a Frenkel configuration, while the elements ω_{AB} and ω_{BA} describe the probability of charge transfer electronic configurations. The results of our calculations are given in Table S3 and summarized visually in **Figure 5**.

The optical properties of a dimer are determined by spatial orientation of individual transition dipoles. The aggregation of obPDI-1 monomers arranges chromophores in a slipped H-aggregate configuration (Figure 5a) with the supramolecular S_1 (2.26eV) and S_2 (2.32eV) states given by a linear combination of localized states. For state S_1, ω_{AA} and ω_{BB} were 0.49 and 0.49 and for S_2 0.40 and 0.40. The complete compensation of antiparallel monomeric transition dipoles results in a net zero transition moment of the S_1 state, causing it to be optically dark. Thus, the light emission from this state occurs in the Herzberg-Teller regime, which explains the long fluorescence lifetime of the obPDI-1 aggregate, as shown in Figure 3a. It is also noteworthy a relatively large energy gap of 0.3 eV exists between the S_2 and a pair of CT states (2.60 and 2.68 eV).

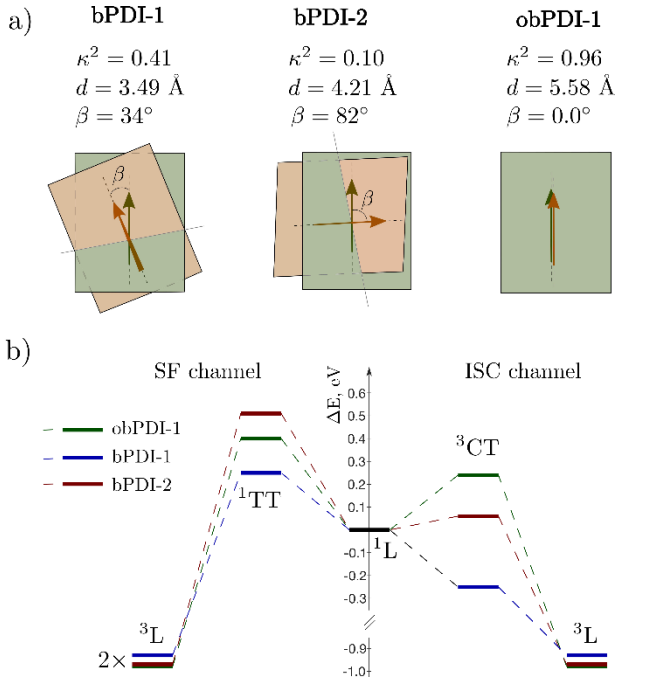

Figure 5. a) Mutual arrangement of molecular planes and monomeric transition dipoles; κ - orientation factor; d-intermolecular distance; ß - angle between transition dipoles. (b) Excited-states diagram illustrating two ACQ channels in the aggregated class of bPDIs. The bright state energy is taken as the origin.

Molecules in aggregated bPDI-2 form a cofacial configuration with perylene cores twisted by 82° with respect to each other (Figure 5a). A relatively small Förster orientation parameter (κ = -0.31) partially eliminates the interchromophore coupling resulting in nearly degenerate S_1 and S_2 states (2.32 and 2.33eV). In this case the S_1 and S_2 are described to a large extent by Frenkel components (ω_{BB} =0.90 for S1 and ω_{AA} =0.88 for S_2), which are approximately equally coupled to the ground state by an electric dipole. For the aggregated bPDI-2, the CT excitons (forming the S_3 and S_4 states) are higher in energy by about 0.1eV and 0.16eV respectively.

The DFT/MRCI spectrum of bPDI-1 dimer reveals that the Frenkel-like states, i.e. the S_1 (2.10 eV) and S_4 (2.40 eV), encapsulate S_2 (2.24 eV) and S_3 (2.32 eV), which show CT character (ω_{AB} =0.80 for S_2 and ω_{BA} = 0.82 for S_3). The partial distribution of the oscillator strengths f(L) (see Table S3) of the Frenkel S_1 and S_4 states closely resembles the case of H-aggregate (as in obPDI-1), in that the S_1 state has a lower capacity to absorb or emit photons compared to the higher energy S_4 state. Therefore, the existence of the low-lying CT states can be significant for this aggregate.

Previous studies have shown that low-lying CT states can open non-radiative decay pathways, leading to ϕ_{PL} decrease.[48, 49] Moreover, it has been reported that PDI derivatives can show distinct ability to undergo slow singlet fission (SF),[50, 51] which is mediated by the TT electron configuration. In bPDI-1/bPDI-2/obPDI-1 aggregates, the TT state is energetically higher than the brightest optically accessible state by 0.25/0.5/0.4 eV

respectively, see state S_5 in Table S3. This makes SF endothermic for the particular dimer configurations as drawn in Figure 5b. Nonetheless, the singlet-to-triplet conversion can be promoted by means of intersystem crossing (ISC), which can be brought about by non-zero spin-orbit coupling between nearly resonant ^{1}L and ^{3}CT states.[49, 52] These criteria are met in the aggregated bPDI-1, where the ^{3}CT states (T_3 and T_4) and the optically bright 1L state (S_4) differ by ~0.2eV with a SO coupling of 0.2–0.4 cm^{-1} (see Figure 5b).

Overall the quantum chemical calculations suggest that the SF process is unlikely to be the major energy loss mechanism in the aggregate class of bPDIs. However, ISC is a feasible non-radiative pathway in the bPDI-1 dimer, but not in bPDI-2 and obPDI-1. The photophysical properties of the H-aggregate and exothermic ISC explain the lowest ϕ_{PL} in bPDI-1 among the aggregate class of bPDIs. In contrast, the spatial orientation of monomers in the bPDI-2 aggregate causes high optical activity of the lowest singlet excited state. Its large oscillator strength enables a high probability of photon emission and exciton transfer to neighboring chromophores. This makes emission properties of the bPDI-2 dimer superior to the other aggregated species.

Combining Molecular Aggregation and Insulation

To further improve the ϕ_{PL} of the bPDI series at an extremely high fluorophore concentration, we prepared a fluorophore system that consisted of both the insulation and aggregation fractions by blending bPDI-2 and obPDI-4 together. The desired combination provided a well-defined FRET system that consisted of the monomeric donor and aggregated emitters. To the best of our knowledge, this is the first reported donor-emitter FRET system based on a blend of monomers and aggregates with the same fluorophore core structure that enhances the overall ϕ_{PL}.

The absorption spectrum of bPDI-2 overlaps significantly with the monomeric emission of obPDI-4 (Figure 6b), indicating the possibility of efficient FRET. With 10 mM of bPDI-2 and 120 mM of obPDI-4 present, the emission of the sample resembled that of 10 mM bPDI-2 only indicating significant quenching of obPDI-4 emission (Figures 6c and S6). The ϕ_{PL} of the mixed sample was 72% compared to 40% for obPDI-4 only (Figure 4b and 6d). When the concentration of bPDI-2 was increased to 20 mM, the ϕ_{PL} of this blend was enhanced to 85%, which is close to the ϕ_{PL} of bPDI-2 at 20 mM alone (~90%[1]) and higher than the best ϕ_{PL} of bPDIs at 120 mM in PMMA matrix. As the monomeric bPDI-2 and obDPI-4 have almost identical absorption and emission spectra, they can be considered the same PDI fluorophore, leading to a total combined concentration of PDI of 140 mM in the PMMA matrix. By introducing the highly emissive aggregates with the monomeric fluorophores, we successfully achieved a ϕ_{PL} of 85% in a PDI-based FRET system. This is amongst the highest ϕ_{PL} reported for organic fluorophores emitting over a similar wavelength range at 140 mM (~20% w/w).[53-55]

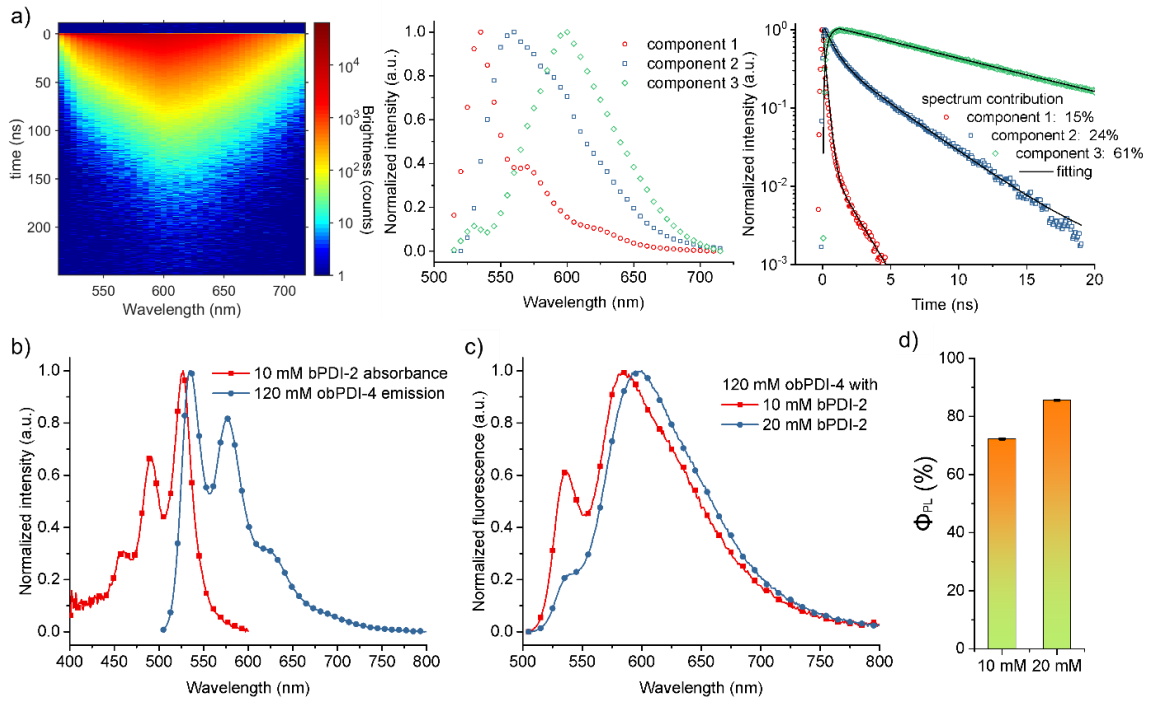

Figure 6. a) Time-resolved emission data from a blend of obPDI-4 and bPDI-2 (120 mM/20 mM in PMMA matrix) together with the spectral and temporal deconvolution via MCR-ALS. b) the spectral overlap between the absorption of 10 mM bPDI-2 and emission of 120 mM obPDI-4 in PMMA matrix. c) the emission spectra of the obPDI-4/bDPI-2 blends and d) the ϕ_{PL} of the obPDI-4/bDPI-2 mixtures.

As the concentration of bPDI-2 was much lower than obPDI-4, the incident light was mainly absorbed by obPDI-4 (>85% contribution for the 120:20 mM sample) with the excitation energy then transferred to bPDI-2 via the FRET process. The

spectral decomposition of the time-resolved fluorescence spectrum of the obPD-4 / bPDI-2 mixture (120:20 mM, **Figure 6a**) showed three components contributing to the overall fluorescence spectrum, namely the monomeric residue from obPDI-4 and bPDI-2 (component 1, 15%), the aggregates of obPDI-4 (component 2, 24%) and the aggregates of bPDI-2 (component 3, 61%). The fluorescence spectra of component 1 and 2 matched the spectral decomposition from the pure obPDI-4 samples (Figure 3a) at the same concentration, while the spectrum of component 3 also matched the emission of bPDI-2 at 20 mM in a PMMA matrix (Figure S6). As expected, the average fluorescence lifetime of component 1 (τ = 0.24 ns, Table S2) was much shorter than the average fluorescent lifetime of obPDI-4 in dilute solution (τ = 3.89 ns, Table S1). Considering the high ϕ_{PL} of the sample mentioned previously, component 1 was less likely quenched by non-radiative pathways. Component 3 showed a growth in intensity on a time scale (τ_g = 0.36 ns) very similar to the short decay of component 1 (τ_1 = 0.21 ns, Table S2), suggesting the formation of component 3 corresponded to the quenching of component 1. As the emission from component 3 dominated the fluorescence spectrum of the obPDI-4/bPDI-2 mixture, one can conclude that bPDI-2 efficiently quenched excited obPDI-4. This reduced energy loss by non-radiative pathways leads to the high ϕ_{PL} observed for this fluorophore blend system.

Conclusions

In conclusion, this study provides a new design approach for PDI derivatives with high ϕ_{PL}. Two new PDI derivatives were synthesized and characterized to establish the relation between ϕ_{PL} and the molecular structures. Both the well-insulated obPDI-4 and obPDI-1 aggregates showed only modest ϕ_{PL} among all reported bPDIs, which clearly suggested neither approach was sufficient to prevent the ϕ_{PL} decreasing by concentration quenching. Instead, PDIs with a combination of both molecular insulation and aggregation characteristics demonstrated the best ϕ_{PL} at high concentration both in PMMA matrix and in the neat solid-state. The DFT/MRCI calculations suggested that the spatial orientation of monomers in bPDI-2 aggregate enabled a high probability of photon emission and exciton transfer to neighboring chromophores. In addition, the endothermic SF and ISC channels explained why emission properties of bPDI-2 aggregates were superior to those in the other aggregated species. The formation of a small amount of emissive aggregates was the main reason the Φ_{PL} values of bPDI-2 and bPDI-4 were superior in the bPDI series. In addition, a blend of obPDI-4 and bPDI-2 was prepared resulting in a monomer-aggregate FRET system with enhanced ϕ_{PL}. The resulting FRET system gave the best ϕ_{PL} among all bPDIs at high concentration in PMMA matrix. Our future research will focus on the design of new fluorophores that utilize both molecular insulation and aggregation characteristics to enhance ϕ_{PL}.

Conflicts of interest

There are no conflicts to declare. The authors declare no competing financial interest.

Acknowledgements

This work was made possible by support from the Australian Renewable Energy Agency, which funds the project grants within the Australian Centre for Advanced Photovoltaics (ACAP). This work was also supported by the ARC Centre of Excellence in Exciton Science (CE170100026). BZ is supported by the Albert Shimmins Postgraduate Writing Up Award. We gratefully acknowledge the Australian Synchrotron for beamtime via the Collaborative Access Program (proposal number 13618b).[56]

Notes

Material synthesis, spectroscopy measurement, DFT/MRCI calculation details and X-ray crystallography data (CIF) can be found in the Supporting Information. Supporting Information is available from the Wiley Online Library or from the author.
CCDC 1949530, CCDC 1949529 and CCDC 1949528 contain the supplementary crystallographic data for this paper. These data can be obtained free of charge from The Cambridge Crystallographic Data Centre via www.ccdc.cam.ac.uk/data_request/cif.

References

1. B. Zhang, H. Soleimaninejad, D. J. Jones, J. M. White, K. P. Ghiggino, T. A. Smith and W. W. H. Wong, *Chem. Mater.*, 2017, **29**, 8395-8403.
2. C. Würth, M. Grabolle, J. Pauli, M. Spieles and U. Resch-Genger, *Anal. Chem.*, 2011, **83**, 3431-3439.
3. T. N. Kalyani and S. J. Dhoble, *Renew. Sust. Energy Rev.*, 2012, **16**, 2696-2723.
4. F. Cicoira and C. Santato, *Adv. Funct. Mater.*, 2007, **17**, 3421-3434.
5. P. D. Frischmann, K. Mahata and W.-F. Reviews, *Chem. Soc. Rev.*, 2013, DOI: 10.1039/C2CS35223K.
6. M. G. Debije and P. P. C. Verbunt, *Adv. Energy Mater.*, 2012, **2**, 12-35.
7. J. L. Banal, B. Zhang, D. J. Jones, K. P. Ghiggino and W. W. Wong, *Acc. Chem. Res*, 2017, **50**, 49-57.
8. B. Zhang, P. Zhao, L. J. Wilson, J. Subbiah, H. Yang, P. Mulvaney, D. J. Jones, K. P. Ghiggino and W. W. H. Wong, *ACS Energy Lett.*, 2019, **4**, 1839-1844.
9. G. Chen, W. Li, T. Zhou, Q. Peng, D. Zhai, H. Li, W. Yuan, Y. Zhang and B. Tang, *Adv. Mater.*, 2015, **27**, 4496-4501.
10. W. Yuan, P. Lu, S. Chen, J. W. Y. Lam, Z. Wang, Y. Liu, H. Kwok, Y. Ma and B. Tang, *Adv. Mater.*, 2010, **22**, 2159-2163.
11. A. M. Brouwer, *Pure Appl. Chem.*, 2011, **83**, 2213-2228.
12. R. Jakubiak, C. J. Collison, W. Wan, L. J. Rothberg and B. R. Hsieh, *J. Phys. Chem. A*, 1999, **103**, 2394-2398.
13. M. Noh, T. Kim, H. Lee, C.-K. Kim, S.-W. Joo and K. Lee, *Colloids Surf. A*, 2010, **359**, 39-44.
14. L. F. Ferreira and S. Costa, *J. Lumin.*, 1991, **48**, 395-399.

15. Y. Hong, J. W. Y. Lam and B. Z. Tang, *Chem. Soc. Rev.*, 2011, **40**, 5361-5388.
16. J. Mei, Y. Hong, J. W. Y. Lam, A. Qin, Y. Tang and B. Tang, *Adv. Mater.*, 2014, **26**, 5429-5479.
17. B. Zhang, J. L. Banal, D. J. Jones, B. Tang, K. P. Ghiggino and W. W. H. Wong, *Mater. Chem. Front.*, 2018, **2**, 615-619.
18. Z. Wei, Z.-Y. Gu, R. K. Arvapally, Y.-P. Chen, R. N. McDougald, J. F. Ivy, A. A. Yakovenko, D. Feng, M. A. Omary and H.-C. Zhou, *J. Am. Chem. Soc.*, 2014, **136**, 8269-8276.
19. J. L. Banal, H. Soleimaninejad, F. M. Jradi, M. Liu, J. M. White, A. W. Blakers, M. W. Cooper, D. J. Jones, K. P. Ghiggino, S. R. Marder, T. A. Smith and W. W. H. Wong, *J. Phys. Chem. C*, 2016, **120**, 12952-12958.
20. S.-C. Lo, T. D. Anthopoulos, E. B. Namdas, P. L. Burn and I. D. W. Samuel, *Adv. Mater.*, 2005, **17**, 1945-1948.
21. P. Osswald and F. Würthner, *Chem. Eur. J.*, 2007, **13**, 7395-7409.
22. F. Biedermann, E. Elmalem, I. Ghosh, W. M. Nau and O. A. Scherman, *Angew. Chem. Int. Ed.*, 2012, **51**, 7739-7743.
23. M. Mitsui, H. Fukui, R. Takahashi, Y. Takakura and T. Mizukami, *J. Phys. Chem. A*, 2017, **121**, 1577-1586.
24. Y. Fujiwara, R. Ozawa, D. Onuma, K. Suzuki, K. Yoza and K. Kobayashi, *J. Org. Chem.*, 2013, **78**, 2206-2212.
25. J. Baggerman, D. C. Jagesar, R. A. L. Vallée, J. Hofkens, F. C. De Schryver, F. Schelhase, F. Vögtle and A. M. Brouwer, *Chem. Eur. J.*, 2007, **13**, 1291-1299.
26. M.-J. Lin, Á. J. Jiménez, C. Burschka and F. Würthner, *Chem. Commun.*, 2012, **48**, 12050-12052.
27. C. Haines, M. Chen and K. P. Ghiggino, *Sol. Energy Mater. Sol. Cells*, 2012, **105**, 287-292.
28. Z. Chen, V. Stepanenko, V. Dehm, P. Prins, L. D. A. Siebbeles, J. Seibt, P. Marquetand, V. Engel and F. Würthner, *Chem. Eur. J.*, 2007, **13**, 436-449.
29. T. T. Vu, S. Badré, C. Dumas-Verdes, J.-J. Vachon, C. Julien, P. Audebert, E. Y. Senotrusova, E. Y. Schmidt, B. A. Trofimov, R. B. Pansu, G. Clavier and R. Méallet-Renault, *J. Phys. Chem. C*, 2009, **113**, 11844-11855.
30. A. Reisch, P. Didier, L. Richert, S. Oncul, Y. Arntz, Y. Mély and A. S. Klymchenko, *Nat. Comm.*, 2014, **5**, 4089.
31. I. Medintz and N. Hildebrandt, *FRET-Förster resonance energy transfer: from theory to applications*, John Wiley & Sons, Hoboken, 2013.
32. N. Felorzabihi, P. Froimowicz, J. C. Haley, G. Bardajee, B. Li, E. Bovero, F. C. J. M. van Veggel and M. A. Winnik, *J. Phys. Chem. B*, 2009, **113**, 2262-2272.
33. C. Hippius, I. H. M. van Stokkum, M. Gsanger, M. M. Groeneveld, R. M. Williams and F. Wurthner, *J. Phys. Chem. C*, 2008, **112**, 2476-2486.
34. D. Genovese, S. Bonacchi, R. Juris, M. Montalti, L. Prodi, E. Rampazzo and N. Zaccheroni, *Angew. Chem. Int. Ed.*, 2013, **52**, 5965-5968.
35. Y. Jiang and J. McNeill, *Chem. Rev.*, 2017, **117**, 838-859.
36. K. Trofymchuk, A. Reisch, P. Didier, F. Fras, P. Gilliot, Y. Mely and A. S. Klymchenko, *Nat. Photonics*, 2017, **11**, 657-663.
37. S. Nakazono, S. Easwaramoorthi, D. Kim, H. Shinokubo and A. Osuka, *Org. Lett.*, 2009, **11**, 5426-5429.
38. V. Yasarapudi, L. Frazer, J. Webb, J. Gallaher, A. Macmillan, A. Falber, P. Thordarson and T. W. Schmidt, *J. Phys. Chem. C*, 2018, DOI: 10.1021/acs.jpcc.8b01084.
39. V. Klema and A. Laub, *IEEE Trans. Autom. Control*, 1980, **25**, 164-176.
40. C. F. V. Loan, *SIAM J. Numer. Anal.*, 1976, **13**, 76-83.
41. J. Jaumot, A. de Juan and R. Tauler, *Chemom. Intell. Lab. Syst.*, 2015, **140**, 1-12.
42. S. Yagai, T. Seki, T. Karatsu, A. Kitamura and F. Würthner, *Angew. Chem. Int. Ed.*, 2008, **47**, 3367-3371.
43. D. Chaudhuri, D. Li, Y. Che, E. Shafran, J. M. Gerton, L. Zang and J. M. Lupton, *Nano Lett.*, 2010, **11**, 488-492.
44. A. Schubert, V. Settels, W. Liu, F. Würthner, C. Meier, R. F. Fink, S. Schindlbeck, S. Lochbrunner, B. Engels and V. Engel, *J. Phys. Chem. Lett.*, 2013, **4**, 792-796.
45. R. F. Fink, J. Seibt, V. Engel, M. Renz, M. Kaupp, S. Lochbrunner, H.-M. Zhao, J. Pfister, F. Würthner and B. Engels, *J. Am. Chem. Soc.*, 2008, **130**, 12858-12859.
46. I. Lyskov, M. Kleinschmidt and C. M. Marian, *J. Chem. Phys.*, 2016, **144**, 034104.
47. J. D. Spiegel, I. Lyskov, M. Kleinschmidt and C. M. Marian, *Chem. Phys.*, 2017, **482**, 265-276.
48. D. C. Santra, M. K. Bera, P. K. Sukul and S. Malik, *Chem. Eur. J.*, 2016, **22**, 2012-2019.
49. Z. E. X. Dance, S. M. Mickley, T. M. Wilson, A. B. Ricks, A. M. Scott, M. A. Ratner and M. R. Wasielewski, *J. Phys. Chem. A*, 2008, **112**, 4194-4201.
50. S. W. Eaton, L. E. Shoer, S. D. Karlen, S. M. Dyar, E. A. Margulies, B. S. Veldkamp, C. Ramanan, D. A. Hartzler, S. Savikhin, T. J. Marks and M. R. Wasielewski, *J. Am. Chem. Soc.*, 2013, **135**, 14701-14712.
51. A. K. Le, J. A. Bender and S. T. Roberts, *J. Phys. Chem. Lett.*, 2016, **7**, 4922-4928.
52. Y. Zhao, R. Duan, J. Zhao and C. Li, *Chem. Commun.*, 2018, **54**, 12329-12332.
53. Z. Ning, Z. Chen, Q. Zhang, Y. Yan, S. Qian, Y. Cao and H. Tian, *Adv. Funct. Mater.*, 2007, **17**, 3799-3807.
54. M. Xiao and P. R. Selvin, *J. Am. Chem. Soc.*, 2001, **123**, 7067-7073.
55. N. Zhao, Z. Yang, J. W. Y. Lam, H. H. Y. Sung, N. Xie, S. Chen, H. Su, M. Gao, I. D. Williams, K. Wong and B. Tang, *Chem. Commun.*, 2012, **48**, 8637-8639.
56. N. P. Cowieson, D. Aragao, M. Clift, D. J. Ericsson, C. Gee, S. J. Harrop, N. Mudie, S. Panjikar, J. R. Price, A. Riboldi-Tunnicliffe, R. Williamson and T. Caradoc-Davies, *Journal of Synchrotron Radiation*, 2015, **22**, 187-190.